Image Reconstruction from Data Acquired With an X-Ray Computerized Tomographic System Having Energy-Integrating Detectors

Joseph A. O'Sullivan, Bruce R. Whiting, Donald L. Snyder, and Orville A. Earl

***Abstract*— Detectors used in modern X-ray tomographic systems accumulate the energy of the photons sensed. The statistical description of such data departs from the Poisson-process model often used in developing image-reconstruction algorithms. Our goal in this brief paper is to review a model for data produced by an energy integrating detector and then to give a maximum-likelihood image-reconstruction method consistent with this model.**

***Index Terms*— tomography, computerized tomography, beam hardening, image reconstruction**

I. Introduction

Our group's research on reducing streak artifacts that are present in X-ray tomographic images when high density metallic objects are present in the body has led to our conclusion that a physically accurate data model coupled with a reconstruction algorithm that accommodates the model are crucial for reducing artifacts to an acceptable level [12], [17]. This has caused us to examine more closely the models and assumptions that are used to derive image reconstruction methods [8], [16]. For similar reasons, other research groups have likewise been motivated to reexamine models for X-ray CT data [3]. This paper is an expanded version of [9].

That X-ray sources produce polyenergetic photons and that the constituents of the body have energy dependent attenuation characteristics have long been recognized. Models describing these effects are readily available [1], [2], [14]. When developing image reconstruction algorithms that accommodate these effects, it is common to assume that the data acquired by the tomograph are Poisson distributed [4], [8], [12]. In this instance, each detected photon is treated as a quantum "event" without other attributes, and the data are modeled as an accumulation or counting of events as follows. Let d_m denote the data acquired at the *m*th source-detector position among the M such positions that are present as the scanner acquires a complete set of data for forming a tomographic image,

$$d_m = \int\limits_{y \in \mathcal{Y}_m} \int\limits_{E \in \mathcal{E}_m} N(dy, dE) \tag{1}$$

for $m = 1, 2, \cdots, M$, where $\mathcal{Y}_m$ denotes the region of the measurement or sinogram space, $\mathcal{Y}$, corresponding to the *m*th source-detector position, $\mathcal{E}_m$ is the range of energies that influence these data, and $N(\cdot, \cdot)$ is a Poisson counting process [13] defined on the sinogram-energy space, $\mathcal{Y} \times \mathcal{E}$. The mean-value function of the Poisson process $N(\cdot, \cdot)$ is

$$q(y, E) = I_0(y, E) \exp\left[- \sum_{x \in \mathcal{X}} h(y|x) \mu(x, E) \right], \tag{2}$$

for $(y, E) \in \mathcal{Y} \times \mathcal{E}$, where $I_0(y, E)$ is the combined energy-dependent source flux and detector absorption, $\mathcal{X}$ is the pixelized image space, $h(y|x)$ is the scanner's point-spread function, and $\mu(\cdot, \cdot)$ is the spatially varying, energy-dependent attenuation function that is sought. The data, d_m, are Poisson distributed,

$$\Pr(d_m = n) = \frac{Q_m^n}{n!} e^{-Q_m}, \tag{3}$$

for $n = 0, 1, 2, \cdots$, where the mean number of detection events, Q_m, is given by

$$Q_m = \int\limits_{y \in \mathcal{Y}_m} \int\limits_{E \in \mathcal{E}_m} q(y, E) dy dE. \tag{4}$$

The units of E and $\mu(\cdot, \cdot)$ are generally keV and mm^{-1}, respectively. As in [8], we assume that the attenuation function is in the form of a sum of separable components having nonnegative factors,

$$\mu(x, E) = \sum_{i=1}^{I} \mu_i(E) \, c_i(x), \tag{5}$$

where I is the number of constituents in the scanned volume, and the *i*th constituent has a known attenuation $\mu_i(\cdot)$, in mm^{-1}, that depends only on energy, E, and an unknown, relative partial-density $c_i(\cdot)$ that depends only on position, x. We call functions in this form *admissible* and denote the set of such functions by $\mathcal{U}$. Decompositions of this form are discussed by J. Weaver and A. Huddleston [15] and by J. Williamson, *et al*. [17].

II. Data model for energy-integrating detectors

As noted by Whiting [16], the data acquired by current CT scanners are not Poisson distributed because they result from a polyenergetic photon flux that is converted by the X-ray detectors into secondary energy forms (for example, electrons or

The authors are with Washington University, St. Louis, MO

optical photons) that are electronically integrated into an essentially continuous signal that is then sampled and quantized into a digital value. When the effects of quantization are ignored, the data, d_m, produced by the *m*th detector are more accurately modeled in terms of a compound Poisson process as

$$d_m = \int\limits_{y\in\mathcal{Y}_m} \int\limits_{E\in\mathcal{E}_m} EN(dy, dE), \tag{6}$$

which replaces the expression for d_m in (1). The characteristic function for d_m, defined by

$$M_{d_m}(jv) \triangleq \bar{E}\left[e^{jvd_m}\right], \tag{7}$$

where $\bar{E}[\cdot]$ is the expectation operator, is readily determined to be (see eq. (4.8) in [13])

$$M_{d_m}(jv) = e^{Q_m[M_E(jv)-1]}, \tag{8}$$

where $M_E(jv)$ is the characteristic function of the energies of detected photons. By inverse Fourier transformation of $M_{d_m}(jv)$, the probability density of d_m is given by

$$p_{d_m}(D_m) = \sum_{n=0}^{\infty} \frac{Q_m^n}{n!} p_E^{n\otimes}(D_m) e^{-Q_m}, \tag{9}$$

in which $p_E(\alpha)$ is the probability density of photon energies, and the superscript "$n\otimes$" denotes n-fold autoconvolution. We note that if each photon incident on the detector contributes unit energy to the data, then $p_E(\alpha) = \delta(\alpha - 1)$ and $p_E^{n\otimes}(\alpha) = \delta(\alpha - n)$, so that (9) and (3) become equivalent.

It is of interest to introduce the energy spectrum of detected photons, $q_m(E)$, into the data density (9), where

$$q_m(E) = \int\limits_{y\in\mathcal{Y}_m} q(y, E)dy. \tag{10}$$

Then,

$$p_E(\alpha) = \frac{q_m(\alpha)}{\int\limits_{E\in\mathcal{E}_m} q_m(E)\, dE} = \frac{q_m(\alpha)}{Q_m}. \tag{11}$$

Substitution into (9) then yields the following expression for the probability density of the data, d_m:

$$p_{d_m}(D_m) = \sum_{n=0}^{\infty} \frac{1}{n!} q_m^{n\otimes}(D_m) e^{-Q_m}. \tag{12}$$

The summation in (12) can be thought of as a weighted series of terms, each term representing the spectrum corresponding to n total events (formed by n autoconvolutions of the original spectrum), with a weighting corresponding to the probability for integer n of a Poisson process of mean Q_m.

It is straightforward to compute the probability densities corresponding to representative clinical CT scan conditions. Using available X-ray spectra and material attenuation coefficients, the spectrum of quanta transmitted through an object and interacting with a detector can be obtained. For a given scan protocol (tube current, integration time, collimation and active detector area), the total X-ray flux is determined, allowing an estimate of the probability density from (12). Fig. 1 shows a representative example. In comparing the theoretical model predictions to experimental data, measurements were performed on phantom objects of uniform materials constructed in simple geometries to determine the noise characteristics of clinical scanners. In these real devices, processes (e.g., electronic noise, beam hardening corrections, scattered radiation) present in addition to X-ray quantum noise contribute to signal statistics and must be included in data analysis. Fig. 1 shows the fit of the experimental data to the model we have proposed here.

The joint probability density of the data acquired at all M source-detector positions, $\boldsymbol{d} \equiv (d_1, d_2, \cdots, d_M)$, is simply the product of the individual densities because the distinct source-detector positions sample from the Poisson process $N(\cdot,\cdot)$, which has independent increments. Thus:

$$p_{\boldsymbol{d}}(\boldsymbol{D} : \mu) = \prod_{m=1}^{M} p_{d_m}(D_m), \tag{13}$$

where we indicate explicitly that this joint density is a functional of the attenuation $\mu(\cdot,\cdot)$ by virtue of (2), (10), and (12).

III. Image Reconstruction Problem

The image reconstruction problem is to form an admissible estimate (i.e., an estimate in the form (5)) of the attenuation function $\mu(\cdot,\cdot)$ given the data, $\boldsymbol{d}$. In particular, we seek an estimate $\hat{\mu}(x, E)$ of $\mu(x, E)$, for each $(x, E) \in \mathcal{X} \times \mathcal{E}$, that maximizes the data loglikelihood functional $\ell(\mu) = \ln p_{\boldsymbol{d}}(\boldsymbol{D} : \mu)$ subject to the constraint that $\hat{\mu}(\cdot,\cdot) \in \mathcal{U}$. From (12) and (13),

$$\hat{\mu}(x, E) = \arg\max_{\mu\in\mathcal{U}} \sum_{m=1}^{M} \ln\left[\sum_{n=0}^{\infty} \frac{1}{n!} q_m^{n\otimes}(D_m : \mu)\right], \tag{14}$$

where $q_m(D_m : \mu) \equiv q_m(D_m)$ is given in (10) with $E = D_m$. Direct maximization of this loglikelihood functional is difficult, so we have developed an iterative approach for producing maximizers numerically.

IV. Image Reconstruction Method

Our approach for developing a reconstruction method with data derived from energy integrating detectors is based on an expectation-maximization algorithm. Take as the complete data the photon events incident on each source-detector combination, including their energies. These form the Poisson process $N(\cdot,\cdot)$ with mean-value function $q(\cdot,\cdot)$ given in (2). The complete data loglikelihood functional is

$$\ell_{\mathrm{cd}}(\mu) = \sum_{m=1}^{M} \left[\int\limits_{\mathcal{Y}_m} \int\limits_{\mathcal{E}_m} \ln q(y, E) N(dy, dE) - \int\limits_{\mathcal{Y}_m} \int\limits_{\mathcal{E}_m} q(y, E) dy dE\right]. \tag{15}$$

Each iteration of the expectation-maximization algorithm requires an expectation step and a maximization step.

A. Expectation Step

For the expectation step, a current estimate of the attenuation function $\mu(\cdot,\cdot)$ is used to compute the expected value of the complete-data loglikelihood functional given the data d_m. Denote by $Q\left(\mu|\hat{\mu}^{(k)}\right)$ the conditional expectation of $\ell_{\rm cd}\left(\mu\right)$ given the data $\boldsymbol{d} \equiv (d_1, d_2, \cdots, d_M)$ and the stage-k admissible estimate $\hat{\mu}^{(k)}(y,E)$ of $\mu(y,E)$,

$$Q\left(\mu|\hat{\mu}^{(k)}\right) = \bar{E}\left[\ell_{\rm cd}\left(\mu\right)|\boldsymbol{d},\hat{\mu}^{(k)}\right]. \tag{16}$$

Then, from (15),

$$Q\left(\mu|\hat{\mu}^{(k)}\right) = \sum_{m=1}^{M}\int_{\mathcal{Y}_m}\int_{\mathcal{E}_m}\left[p\left(y,E:\hat{\mu}^{(k)}\right)\ln q(y,E:\mu) - q(y,E:\mu)\right]dydE, \tag{17}$$

where $p\left(y,E:\hat{\mu}^{(k)}\right)$ is the intensity of the Poisson process $N(\cdot,\cdot)$ given $\boldsymbol{d}$ and $\hat{\mu}$. The function $p\left(y,E:\hat{\mu}^{(k)}\right)$ that is needed to complete the definition of the expectation step is derived in the Appendix and is given by

$$p\left(y,E:\mu\right) = q(y,E:\mu)\frac{p_{d_m}\left(D_m - E:\mu\right)}{p_{d_m}\left(D_m:\mu\right)}, \tag{18}$$

for $(y,E) \in \mathcal{Y}_m \times \mathcal{E}_m$, in which $p_{d_m}(D_m:\mu)$ is given in (12) with its dependence on μ indicated explicitly.

If each photon incident on the detector contributes unit energy to the data, then $p_E(\alpha) = \delta(\alpha - 1)$,

$$p_{d_m}\left(\alpha - 1:\mu\right) = \frac{\alpha}{Q_m}p_{d_m}\left(\alpha:\mu\right), \tag{19}$$

and

$$p(y,E:\mu) = \frac{\alpha}{Q_m}q(y,E:\mu), \tag{20}$$

which is the expression for $p\left(y,E:\mu\right)$ used in the alternating maximization method developed by J. O'Sullivan and J. Benac [8] for forming a maximum-likelihood estimate of $\mu(x,E)$ under the assumption that sinogram data are Poisson distributed. The expression (18) is the required modification when an energy-integrating detector is used.

Note that I. Elbakri and J. Fessler [5] describe an efficient algorithm for computing the likelihood function $p_{\,d_m}(E)$ needed in the expectation step of the EM algorithm that might be used. Their method is based on a saddle-point approximation of the inverse transform of the moment-generating function (8).

B. Maximization Step

Given $p\left(y,E:\hat{\mu}\right)$, the maximization step is identical to that by J. O'Sullivan and J. Benac [8]. A key portion of that derivation is described here.

The maximization of $Q(\mu|\hat{\mu})$ over μ is notoriously difficult, with many approximations proposed in the literature. More specifically, substitution of q using the form of μ in (5) into the expression for $Q(\mu|\hat{\mu})$ in (17), and dropping terms that do not depend on $\{c_i(x), i = 1,2,\ldots,I\}$ yields

$$Q\left(\mu|\hat{\mu}^{(k)}\right) = \sum_{m=1}^{M}\int_{\mathcal{Y}_m}\int_{\mathcal{E}}\left[-p\left(y,E:\hat{\mu}^{(k)}\right)\sum_{x\in\mathcal{X}}h(y|x)\sum_{i=1}^{I}\mu_i(E)c_i(x) - I_0(y,E)\exp\left(-\sum_{x\in\mathcal{X}}h(y|x)\sum_{i=1}^{I}\mu_i(E)c_i(x)\right)\right]dydE. \tag{21}$$

The difficulty in the maximization is from the last term. That term may be rewritten as a perturbation from the previous estimate as

$$-\int_{\mathcal{Y}}\int_{\mathcal{E}}q(y,E:\hat{\mu}^{(k)})\exp\left(-\sum_{x\in\mathcal{X}}h(y|x)\times\sum_{i=1}^{I}\mu_i(E)(c_i(x) - \hat{c}_i^{(k)}(x))\right)dydE. \tag{22}$$

This term is concave in the $\{c_i(x)\}$. To obtain an analytic form for the update, this term is lower bounded by another concave function of the $\{c_i(x)\}$. This auxiliary functional is analogous to the formulation of the expectation-maximization algorithm's use of the complete data loglikelihood functional to maximize the incomplete data loglikelihood functional.

The auxiliary functional may be obtained most simply by introducing the ratio $Z_i(x)/Z_i(x)$ into the exponent where $Z_i(x)$ is chosen to satisfy

$$\sum_{x\in\mathcal{X}}h(y|x)\sum_{i=1}^{I}\mu_i(E)\frac{1}{Z_i(x)} \le 1, \tag{23}$$

for all (y,E). Then a version of Jensen's inequality applied to the concave function $-qe^{-t}$ yields

$$-\int_{\mathcal{Y}}\int_{\mathcal{E}}q(y,E:\hat{\mu}^{(k)})\exp\left(-\sum_{x\in\mathcal{X}}h(y|x)\times\sum_{i=1}^{I}\mu_i(E)(c_i(x) - \hat{c}_i^{(k)}(x))\right)dydE$$
$$\ge -\sum_{i=1}^{I}\sum_{x\in\mathcal{X}}\frac{1}{Z_i(x)}\hat{b}_i^{(k)}(x)\exp\left(-Z_i(x)(c_i(x) - \hat{c}_i^{(k)}(x))\right), \tag{24}$$

where $\hat{b}$ is the backprojection of q

$$\hat{b}_i^{(k)}(x) = \int_{\mathcal{Y}}\int_{\mathcal{E}}q(y,E:\hat{\mu}^{(k)})h(y|x)\mu_i(E)dydE. \tag{25}$$

Defining $\hat{a}_i^{(k)}(x)$ to be the backprojection of $p\left(y,E:\hat{\mu}^{(k)}\right)$ (substitute p for q in (25), the maximization step using the auxiliary functional becomes simply to maximize

$$\sum_{i=1}^{I}\sum_{x\in\mathcal{X}}\left[-\hat{a}_i^{(k)}(x)c_i(x)\right.$$

$$-\frac{1}{Z_i(x)}\hat{b}_i^{(k)}(x)\exp\left(-Z_i(x)(c_i(x)-\hat{c}_i^{(k)}(x))\right)\Bigg]. \quad (26)$$

This maximization is straightforward, yielding

$$\hat{c}_i^{(k+1)}(x)=\hat{c}_i^{(k)}(x)-\frac{1}{Z_i(x)}\ln\frac{\hat{a}_i^{(k)}(x)}{\hat{b}_i^{(k)}(x)}. \quad (27)$$

Successive iterates of this algorithm are guaranteed not to decrease the loglikelihood functional and, generally, to increase it. This follows because the maximization step involves the use of a surrogate function and optimization transfer; see J. Fessler [6] and K. Lange, *et al*. [7].

C. The Image Reconstruction Algorithm

Combining the expectation and maximation steps results in the following image reconstruction algorithm.

---

step 0. (initialize) Set $k=0$, select initial conditions $\hat{c}_i^{(0)}(x)$, $x\in\mathcal{X}$, for $i=1,2,\cdots,I$. Evaluate

$$\hat{\mu}^{(0)}(x,E)=\sum_{i=1}^{I}\mu_i(E)\,\hat{c}_i^{(0)}(x) \quad (28)$$

and

$$\hat{q}^{(0)}(y,E)=I_0(y,E)\exp\left[-\sum_{x\in\mathcal{X}}h(y\,|x)\,\hat{\mu}^{(0)}(x,E)\right]. \quad (29)$$

step 1. Substitute $\hat{\mu}^{(k)}(x,E)$ into (4) and (10) to obtain

$$\hat{Q}_m^{(k)}=\int\limits_{y\in\mathcal{Y}_m}\int\limits_{E\in\mathcal{E}_m}\hat{q}^{(k)}(y,E)dydE \quad (30)$$

and

$$\hat{q}_m^{(k)}(E)=\int\limits_{y\in\mathcal{Y}_m}\hat{q}^{(k)}(y,E)dy. \quad (31)$$

step 2. Substitute $\hat{Q}_m^{(k)}$ and $\hat{q}_m^{(k)}(E)$ into (12) to obtain

$$\hat{p}_{d_m}^{(k)}(D_m)=\sum_{n=0}^{\infty}\frac{1}{n!}\left[\hat{q}_m^{(k)}(D_m)\right]^{n\otimes}e^{-\hat{Q}_m^{(k)}}, \quad (32)$$

and then evaluate

$$\hat{p}^{(k)}(y,E)=\hat{q}^{(k)}(y,E)\,\frac{\hat{p}_{d_m}^{(k)}(D_m-E)}{\hat{p}_{d_m}^{(k)}(D_m)}, \quad (33)$$

for $(y,E)\in\mathcal{Y}_m\times\mathcal{E}_m$, and $m=1,2,\cdots,M$.

step 3. Evaluate the backprojections

$$\hat{a}_i^{(k)}(x)=\sum_{y\in\mathcal{Y}}\sum_{E\in\mathcal{E}}h(y|x)\,\mu_i(E)\,\hat{p}^{(k)}(y,E) \quad (34)$$

and

$$\hat{b}_i^{(k)}(x)=\sum_{y\in\mathcal{Y}}\sum_{E\in\mathcal{E}}h(y|x)\,\mu_i(E)\,\hat{q}^{(k)}(y,E). \quad (35)$$

step 4. Update estimates of the relative partial densities,

$$\hat{c}_i^{(k+1)}(x)=\hat{c}_i^{(k)}(x)-\frac{1}{Z_i(x)}\ln\frac{\hat{a}_i^{(k)}(x)}{\hat{b}_i^{(k)}(x)}. \quad (36)$$

step 5. Update estimates of the attenuation and intensity functions

$$\hat{\mu}^{(k+1)}(x,E)=\sum_{i=1}^{I}\mu_i(E)\,\hat{c}_i^{(k+1)}(x) \quad (37)$$

and

$$\hat{q}^{(k+1)}(y,E)=I_0(y,E)\exp\left[-\sum_{x\in\mathcal{X}}h(y\,|x)\,\hat{\mu}^{(k+1)}(x,E)\right]. \quad (38)$$

step 5. Check for convergence. Exit if converged. Otherwise, increment k, $k\leftarrow k+1$, and return to step 1.

V. Discussion and Conclusions

A new iterative algorithm is proposed for transmission tomography that takes into account energy-dependent detectors. X-ray detectors often convert the energy from X-ray photons into a secondary energy form that is detected. This conversion is energy dependent. The alternating minimization algorithm that is described here generalizes the alternating minimization algorithm derived by O'Sullivan and Benac [8] to accommodate energy dependence of X-ray sources and object attenuation by employing a compound Poisson process model. There are other detector effects that are not included in this model. For example, detectors that sense a single X-ray photon by producing a cascade of secondary photons or electrons might be modeled as an avalanche process [11] or a filtered Poisson process [13]. I. Elbakri and J. Fessler [4] consider such effects for X-ray tomography, but how significant they are in producing quantitative image reconstructions remains an area for future exploration.

Equation (32) in Step 2 of the reconstruction algorithm requires an infinite summation of weighted autoconvolutions, so some type of approximation is required to perform a reconstruction using the algorithm. Truncating the summation to a finite number of terms is one possible approach, but further study will be needed to relate the number of terms retained to the accuracy of a resulting reconstruction. Another alternative is to use a saddle-point approximation along the lines in [5].

The reconstruction we have described yields an estimate of each of the I components in (5) from data in a single sinogram. The accuracy of the estimates will be influenced by the number of components, the energy spectrum of the source, the energy-dependence of the components, and other factors. The reconstruction problem is underdetermined even when there is only a single component, so some form of regularization is incorporated in an implementation. Appropriate forms of regularization for reconstructing multiple components from a single sinogram remains an area for further study. An alternative is to acquire sinograms at multiple source-energy settings. Preliminary results along this line are presented by J. O'Sullivan, J. Benac, and J. Williamson [10].

Experiments are planned to assess the importance of accounting for this energy dependence in practical situations.

VI. Acknowledgments

This work was supported in part by the National Institutes of Health under research grant R01CA75371 from the National Cancer Institute of the National Institutes of Health, (J. Williamson, P. I.) and in part by the Boeing Foundation.

References

[1] J. M. Boone and A.E. Chavez, "Comparison of x-ray cross sections for diagnostic and therapeutic medical physics," *Med. Phys.*, Vol. 23, No. 12, pp. 1997-2005, 1996.

[2] J. M. Boone, "X-ray Production, Interaction, and Detection in Diagnostic Imaging," pp. 1-77 in *Handbook of Medical Imaging*, J. Beutel, H.L. Kundel, and R.L. VanMetter, Editors, 2000, SPIE: Bellingham, Washington.

[3] B. DeMan, J. Nuyts, P. Dupont, G. Marchal, and P. Suetens, "Metal streak artifacts in X-ray computed tomography: a simulation study," Proc. IEEE Nuclear Science Symp. and Medical Imaging Conf., Toronto, Canada, 1998.

[4] I. A. Elbakri and J. A. Fessler, "Statistical X-ray computed tomography image reconstruction with beam hardening correction," *Proc. SPIE 4322, Medical Imaging 2001: Image Processing*' 2001.

[5] I. A. Elbakri and J. A. Fessler, "Efficient and accurate likelihood for iterative image reconstruction in X-ray computed tomography," Proc. SPIE 5032, Medical Imaging 2003: Image Processing, pp. 1839-50, 2003.

[6] J. A. Fessler, "Statistical image reconstruction methods for transmission tomography," Ch. 1 in: *Handbook of Medical Imaging, Volume 2: Medical Image Processing and Analysis*, M. Sonka and J. M. Fitzpatrick, Editors, SPIE, Bellingham, 2000.

[7] K. Lange, D. R. Hunter, and I. Yang, "Optimization transfer using surrogate objective functions," *Journal of Computational Graphics and Statistics*, Vol. 9, No. 1, pp. 1-20, March 2000.

[8] J. A. O'Sullivan and J. Benac, "Alternating minimization algorithms for transmission tomography," *IEEE Transactions on Medical Imaging*, 2004 (in review).

[9] J. A. O'Sullivan, D. L. Snyder, and B. R. Whiting, "Alternating minimization algorithms for transmission tomography using energy detectors," Proc. Thirty-Sixth Asilomar Conference on Signals, Systems, and Computers, Asilomar, CA, November 3-6, 2002.

[10] J. A. O'Sullivan, J. Benac, and J. Williamson, "Alternating minimization algorithm for dual energy X-ray CT," Proc. of IEEE International Symposium on Biomedical Imaging, pp. 579-582, Arlington, Va., April 15, 2004.

[11] S. D. Personick, "Receiver design for digital fiber optic communication systems: I and II," *Bell System Technical Journal*, Vol. 52, No. 6, pp. 843-874 and 875-886, 1973.

[12] D. L. Snyder, J. A. O'Sullivan, B. R. Whiting, R. J. Murphy, J. Banec, J. A. Cataldo, D. G. Politte, and J. F. Williamson, "Deblurring subject to nonnegativity constraints when known functions are present, with application to object-constrained computerized tomography," *IEEE Transactions on Medical Imaging*, Vol. 20, pp. 1009-1017, October 2001.

[13] D. L. Snyder and M. I. Miller, *Random Point Processes in Time and Space*, Springer-Verlag, New York, 1991.

[14] M. M. Ter-Pogossian, *The Physical Aspects of Diagnostic Radiology*, Harper & Row, New York, 1969.

[15] J. B. Weaver and A. L. Huddleston, Attenuation coefficients of body tissues using principal-components analysis, *Med. Phys.*, Vol. 12, pp. 4045, 1985.

[16] B. R. Whiting, "Signal statistics of X-ray computed tomography," Proc. SPIE Conference on *Medical Imaging 2002: Physics of Medical Imaging*, Vol. 4682 (L. Antonuk and M. Yaffe, Editors), San Diego CA, February 2002.

[17] J. F. Williamson, B. R. Whiting, J. Benac, R. J. Murphy, J. A. O'Sullivan, D. G. Politte, and D. L. Snyder, "Prospects for quantitative computed tomography imaging in the presence of foreign metal bodies using statistical image reconstruction," *Medical Physics*, Vol. 29, No. 10, pp. 2404-2418, October 2002.

VII. Appendix: derivation of (17) and (18)

From (4), (15), and (16),

$$Q\left(\mu|\hat{\mu}^{(k)}\right) = \sum_{m=1}^{M} \bar{E}\left[\ell_m|\boldsymbol{d}, \hat{\mu}^{(k)}\right] - Q_m, \qquad (39)$$

where

$$\ell_m = \int\limits_{\mathcal{Y}_m}\int\limits_{\mathcal{E}_m} \ln q\left(y,E\right) N\left(dy,dE\right). \qquad (40)$$

To evaluate the conditional expectation of ℓ_m, consider the joint characteristic function of d_m and ℓ_m, defined by

$$M\left(jv_d, jv_\ell\right) = \bar{E}\left[e^{j\left(v_d d_m + v_\ell \ell_m\right)}\right]. \qquad (41)$$

If n is the number of detection events in $\mathcal{Y}_m \times \mathcal{E}_m$, then

$$\bar{E}\left[e^{j\left(v_d d_m + v_\ell \ell_m\right)}\,|n\right] = \left[\int\limits_{\mathcal{Y}_m}\int\limits_{\mathcal{E}_m} \frac{q(y,E)}{Q_m} e^{j\left(v_d E + v_l \ln q(y,E)\right)} dydE\right]^n \qquad (42)$$

because the event locations, (y, E), occur as if they are independent and identically distributed random variables with probability density $q(y,E)/Q_m$. Then

$$\begin{aligned} &M\left(jv_d, jv_\ell\right) \\ &= \sum_{n=0}^{\infty} \frac{Q_m^n}{n!} e^{-Q_m} \left[\int\limits_{\mathcal{Y}_m}\int\limits_{\mathcal{E}_m} \frac{q(y,E)}{Q_m} e^{j\left(v_d E + v_\ell \ln q(y,E)\right)} dydE\right]^n \\ &= \exp\left[-Q_m + \int\limits_{\mathcal{Y}_m}\int\limits_{\mathcal{E}_m} q\left(y,E\right) e^{j\left(v_d E + v_\ell \ln q(y,E)\right)} dydE\right]. \end{aligned} \qquad (43)$$

The conditional expectaton $\bar{E}\left[\ell_m|d_m = D_m\right]$ can be expressed as

$$\begin{aligned} &\bar{E}\left[\ell_m\,|d_m = D_m\right] \\ &= \frac{\int_{-\infty}^{\infty} L p_{d_m,l_m}(D_m,L) dL}{\int_{-\infty}^{\infty} p_{d_m,l_m}(D_m,L) dL} \\ &= \frac{\int_{-\infty}^{\infty} \frac{\partial M\left(jv_d,jv_\ell\right)}{\partial jv_\ell}\big|_{v_\ell=0} e^{-jv_d D_m} dv_d}{\int_{-\infty}^{\infty} M(jv_d,jv_\ell)\big|_{v_\ell=0} e^{-jv_d D_m} dv_d} \\ &= \frac{\int_{-\infty}^{\infty} \left[\int\limits_{\mathcal{Y}_m}\int\limits_{\mathcal{E}_m} q(y,E)\ln q(y,E) e^{jv_d E} dydE\right] M(jv_d,0) e^{-jv_d D_m} dv_d}{\int_{-\infty}^{\infty} M(jv_d,0) e^{-jv_d D_m} dv_d}. \end{aligned} \qquad (44)$$

After inverse Fourier transformation, the coefficient of $\ln q\left(y,E\right)$ in the numerator of this last expression is seen to be

$$p\left(y,E\right) = q\left(y,E\right)\frac{p_{d_m}\left(D_m - E\right)}{p_{d_m}\left(D_m\right)}, \qquad (45)$$

which is (18). Equation (17) results when μ is replaced by $\hat{\mu}^{(k)}$ and (44) is substituted into (39).

FIGURE

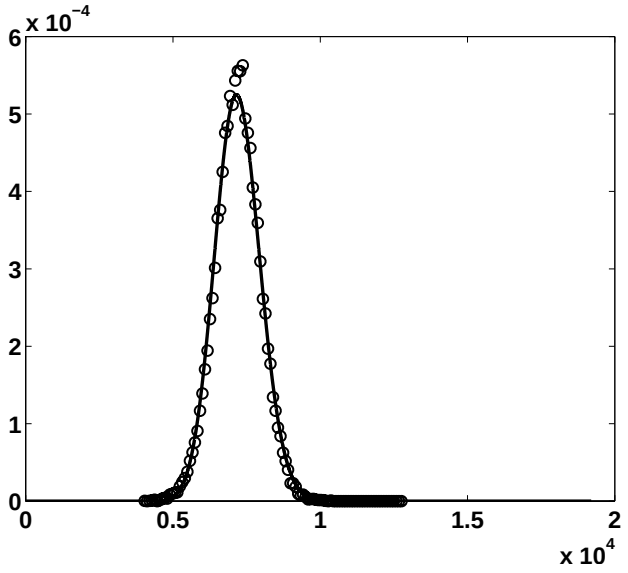

Fig. 1. Theoretical and experimental probability density functions. Abscissa is an arbitrary energy scale, and the ordinate is a probability density value. The solid line represents the probability density for the signal corresponding to that in a 120 kVp X-ray beam passing through 300 mm of polymerized methylmethacrylate, PMMA, with tube current of 150 mA, 1 second gantry rotation, and 1 mm collimation in a Siemens Somatom Plus 4 scanner, corresponding to an incident exposure of $534,000$ quanta per measurement. Experimental points ('o') are relative frequencies of measurements from detectors located in rays passing through 300 mm chords (total attenuation = 6.5) of a PMMA cylinder.

FIGURE CAPTION

Theoretical and experimental probability density functions. Abscissa is an arbitrary energy scale, and the ordinate is a probability density value. The solid line represents the probability density for the signal corresponding to that in a 120 kVp X-ray beam passing through 300 mm of polymerized methylmethacrylate, PMMA, with tube current of 150 mA, 1 second gantry rotation, and 1 mm collimation in a Siemens Somatom Plus 4 scanner, corresponding to an incident exposure of $534,000$ quanta per measurement. Experimental points ('o') are relative frequencies of measurements from detectors located in rays passing through 300 mm chords (total attenuation = 6.5) of a PMMA cylinder.